Spectrochimica Acta Part A: Molecular and Biomolecular Spectroscopy 320 (2024) 124655

Contents lists available at ScienceDirect

Spectrochimica Acta Part A:
Molecular and Biomolecular Spectroscopy

journal homepage: www.journals.elsevier.com/spectrochimica-acta-part-a-molecular-and-biomolecular-spectroscopy

Rapid identification and quantitative analysis of malachite green in fish via SERS and 1D convolutional neural network

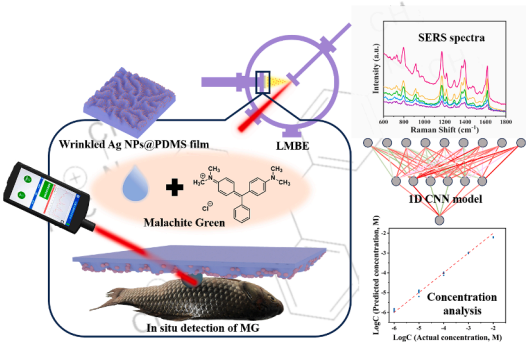
Zhaoyi Zhang, Hefu Li *, Lili Huang, Hongjun Wang, Huijuan Niu, Zhenshan Yang, Minghong Wang *

School of Physical Science and Information Technology, Key Laboratory of Optical Communication Science and Technology of Shandong Province, Liaocheng University, Liaocheng 252000, PR China

HIGHLIGHTS

- A wrinkled Ag NPs@PDMS film was fabricated for in situ SERS detection of malachite green residues.
- High-density and highly available hot spots were present on the PDMS surface.
- The strong adhesion between Ag NPs and PDMS increased the mechanical stability of the substrate.
- 1D CNN model was developed for intelligent analysis of malachite green concentration in fish.

GRAPHICAL ABSTRACT



ARTICLE INFO

Keywords:
SERS
Wrinkled Ag NPs@PDMS film
1D CNN
Malachite green
Point-of-care testing

ABSTRACT

Rapid and quantitative detection of malachite green (MG) in aquaculture products is very important for safety assurance in food supply. Here, we develop a point-of-care testing (POCT) platform that combines a flexible and transparent surface-enhanced Raman scattering (SERS) substrate with deep learning network for achieving rapid and quantitative detection of MG in fish. The flexible and transparent SERS substrate was prepared by depositing silver (Ag) film on the polydimethylsiloxane (PDMS) film using laser molecular beam epitaxy (LMBE) technique. The wrinkled Ag NPs@PDMS film exhibits high SERS activity, excellent reproducibility and good mechanical stability. Additionally, the fast in situ detection of MG residues on fish scales was achieved by using the wrinkled Ag NPs/PDMS film and a portable Raman spectrometer, with a minimum detectable concentration of 10^{-6} M. Subsequently, a one-dimensional convolutional neural network (1D CNN) model was constructed for rapid quantification of MG concentration. The results demonstrated that the 1D CNN quantitative analysis model possessed superior predictive performance, with a coefficient of determination (R^2) of 0.9947 and a mean squared error (MSE) of 0.0104. The proposed POCT platform, integrating a transparent flexible SERS substrate, a portable Raman spectrometer and a 1D CNN model, provides an efficient strategy for rapid identification and quantitative analysis of MG in fish.

* Corresponding authors.
E-mail addresses: lihefu@lcu.edu.cn (H. Li), wangminghong@lcu.edu.cn (M. Wang).

https://doi.org/10.1016/j.saa.2024.124655
Received 29 February 2024; Received in revised form 24 May 2024; Accepted 11 June 2024
Available online 13 June 2024
1386-1425/© 2024 Elsevier B.V. All rights are reserved, including those for text and data mining, AI training, and similar technologies.

1. Introduction

Malachite green (MG), utilized as an aquaculture drug, poses significant threats to human health due to its teratogenic, mutagenic, and carcinogenic effects, leading to its prohibition in most countries [1]. Regrettably, its continued illicit use in the fisheries industry persists due to its low cost, easy accessibility, and efficacy against fungal and parasite infections [2]. Consequently, there is a critical need to develop rapid and sensitive detection methods for determination of MG residues in fish to safeguard human health. While traditional chromatography-based methods offer high sensitivity and accuracy in MG detection, their widespread application is hindered by the necessity for expensive laboratory instruments and intricate pre-treatment processes [3,4]. Contrastingly, the enzyme-linked immunosorbent assays (ELISA) method presents viable alternatives with the advantages of simplicity and selectivity [2]. However, its applicability is confined to qualitative detection. In addition, fluorescence spectroscopy exhibits commendable sensitivity and simplicity for MG determination [5]. Yet, its susceptibility to interference poses a notable limitation in practical applications. Hence, a faster and more straightforward method for detecting MG residues in fish is necessary.

Surface-enhanced Raman scattering (SERS) is a powerful analytical technique, distinguished by its remarkable specificity, ultra-sensitivity, and rapid, non-destructive detection capabilities [6]. It can significantly amplify the feeble Raman signals of analyte molecules that are attached on the SERS substrates, and thus has been widely used in diverse domains, including food safety, environmental monitoring, and biomedicine [7–9]. The main mechanism of the SERS effect is electromagnetic enhancement, rooted in the generation of immensely strong electromagnetic fields localized at nanogaps or edges of metal nanostructures, often referred to as “hot spots” [10]. For sensitive detection of MG residues on fish scales, many researchers have constructed SERS substrates by depositing metal NPs on different materials, such as silicon wafer, graphene, paper and cotton fiber [11–15]. By replacing these rigid or opaque substrates with flexible and transparent alternatives, the scope of SERS applications can be significantly expanded [16,17]. Compared to the swab-sampling method mentioned above, in situ detection strategy is the most convenient, easy, and nondestructive way [18]. The high flexibility of these SERS substrates allows them to be bent or twisted without breaking, enabling them to conform to various surfaces. Furthermore, their transparency facilitates the excitation and collection of signals from both the front and back sides of the substrates, rendering them suitable for in situ SERS detection. Consequently, the flexibility and transparency of SERS substrates make them well-suited for non-destructive and non-invasive detection on curved surfaces, aligning with the requirements for detecting substances like MG in aquatic products [19–21]. Polydimethylsiloxane (PDMS) film has advantages of high transparency, good tensile strength, and a low background Raman scattering [22]. Thus, PDMS film has been widely used for the preparation of transparent and flexible SERS substrates, and exhibited strong practical application potential for in situ detection on the irregular surfaces [23–27]. In the context of in situ detection, the generation of high-quality SERS signals is intricately linked to the accessibility of high-density hot spots for the target molecules [17]. Therefore, a plasmonic nanostructure with an ample supply of hot spots at the surface is imperative for effective SERS enhancement. Moreover, uniformity and reproducibility are also necessary for SERS substrates. Without these attributes, quantitative analysis of target analytes would be an insurmountable challenge. However, it is still challenging to construct highly dense and accessible hot spots on the PDMS surface in a fast, effective, repeatable, and scalable manner.

Moreover, since concentration-dependent SERS spectra cannot directly convey the concentration information of target analytes, it becomes imperative to establish a correlation between the two through chemometric analysis techniques. Notably, recent strides in the development and deployment of machine learning algorithms have propelled the integration of SERS detection and machine learning data analysis. This convergence has steered the SERS technique towards a trajectory of increased automation, intelligence, and visualization [28–31]. Despite these advancements, the performance of traditional machine learning algorithms experiences degradation when dealing with expansive datasets. In recent years, data-driven deep learning methods have garnered widespread attention for their ability to glean features and model intricate relationships from large-scale raw datasets [32–35]. At the forefront of these approaches, the convolutional neural network (CNN) emerges as a classical and extensively employed structure, renowned for its heightened precision and outstanding generalization performance. Its unique architecture seamlessly integrates preprocessing, feature extraction, and identification into a unified framework that can be trained end-to-end without requiring manual tuning. Leveraging SERS spectra datasets, CNNs have demonstrated successful applications in substance classification and quantitative analysis [36–39]. This confluence of SERS and CNN not only underscores the potential for advancing the SERS technique but also signifies a paradigm shift towards heightened automation and intelligence through sophisticated data analysis.

Here, we propose a method for in situ detection and swift quantitative analysis of MG residues on fish scales by concurrently employing a flexible and transparent SERS-active Ag NPs@PDMS film and a 1D CNN regression model (Fig. 1). The wrinkled Ag NPs@PDMS film was fabricated by depositing an Ag film onto the PDMS film using the laser molecular beam epitaxy (LMBE) technique (Fig. 1a). The optimized conditions for creating rolling Ag NPs resulted in the generation of strong and uniform hot spots, enhancing SERS responses significantly. Capitalizing on its exceptional flexibility and transparency, the wrinkled Ag NPs@PDMS film can be adhered to the fish scale surface, allowing for rapid in situ detection of MG through promptly acquired SERS signals. To predict the concentration of MG residues, a 1D CNN model based on SERS spectra was constructed, which can achieve remarkable efficacy in achieving rapid, accurate, and quantitative detection of MG (Fig. 1b). The integration of the developed Ag NPs@PDMS film, coupled with a handheld Raman spectrometer and the 1D CNN quantitative analysis model, holds potential as a point-of-care testing (POCT) platform for on-site, real-time MG sensing in practical scenarios.

2. Materials and methods

2.1. Materials

A high-purity silver target was purchased from Zhongnuo Advanced Material Technology Co., Ltd. Silicon wafers and polydimethylsiloxane (PDMS) were bought from Hangzhou Jingbo Technology Co., Ltd. Rhodamine 6G (R6G) was purchased from Sigma-Aldrich. Malachite Green (MG) was obtained from Aladdin Reagent (Shanghai, China) Co., Ltd. All aqueous solutions were prepared using deionized (DI) water.

2.2. Fabrication of the wrinkled Ag NPs@PDMS film

Initially, the PDMS prepolymer was blended with a curing agent in a 10:1 wt ratio and stirred for 20 min. Subsequently, the mixture underwent a 30-minute degassing process in a vacuum drying oven. Following this, the prepared solution was spin-coated onto a cleaned silicon wafer (2×2 cm^2) at 600 rpm for 8 s, followed by thermal curing at 80 °C for 1 h. After curing, the PDMS film underwent a decoration process with Ag films at varying deposition times (15, 20, 25, and 30 min) via the LMBE growth system. During the deposition process, the pulse energy of the laser beam with wavelength 248 nm was up to 255 mJ, the laser pulse repetition rate was 5 Hz, and the vacuum was 2.0×10^{-4} Pa.

2.3. Characterizations

The morphology and structure of the SERS substrates were

characterized by the atomic force microscopy (Bruker, Dimension Icon SPM) and scanning electron microscopy (SEM, Apero S HiVac). The SERS spectra of R6G were measured using the Renishaw inVia Raman system with a laser of 785 nm (100 % power) and an integration time of 10 s. The SERS spectra of MG were collected using a handheld Raman analyzer (ATR6500, Optosky photoelectric Co., Ltd., China) with a laser of 785 nm (20 mW power).

2.4. SERS measurements

To evaluate the SERS performance of the wrinkled Ag NPs@PDMS film, R6G was selected as a probe molecule to investigate the sensitivity, uniformity, repeatability, mechanical stability and storage stability of the substrates. 10 μL of R6G aqueous solutions were dropped on the SERS substrates and dried naturally. Then, SERS measurements were performed using a Renishaw inVia Raman system. For achieving in situ detection of pesticide residues in actual samples, 20 μL of MG solutions with different concentrations were dropped onto the fish scales and naturally evaporated at room temperature. Then, the wrinkled Ag NPs@PDMS film was attached to the pesticide-contaminated scales with Ag NPs facing the target surface for direct SERS measurements using a portable Raman spectrometer.

2.5. Deep learning analysis

2.5.1. Spectral data augmentation

Developing effective and applicable quantitative models demands an extensive pool of training samples, particularly for deep learning models. The process of amassing such a large dataset is both time-consuming and costly. To ensure the robust training of models, prevent overfitting, and capture diverse forms of deviations from the training samples, diverse data augmentation methods have been introduced. In this study, for augmenting the collected SERS spectra, three independent data augmentation strategies were employed: shift along the x-axis, adding noise, and linear superposition [40,41].

(1) Shift along the x-axis. The original spectrum undergoes random shifting along the x-axis, generating new spectra through the horizontal forward or backward displacement of randomly selected variables within the range of $-5\ cm^{-1}$ to $5\ cm^{-1}$.

(2) Adding noise. This strategy introduces random Gaussian noise, varying in signal-to-noise ratio, to both the original and offset SERS spectra. Adding Gaussian noise with varying signal-to-noise ratios can distort Raman spectra. Lower signal-to-noise ratios make it harder to differentiate signals from noise, potentially leading to data misinterpretation. Spectral resolution may also decrease, impacting peak distinction (Fig. S1). Thus, managing noise levels is crucial for maintaining data integrity.

(3) Linear superposition. New spectra emerge through the linear superposition of multiple SERS spectra at the same concentration, employing a random scaling coefficient with a cumulative value of 1.

Consequently, through this data augmentation process, a total of 2000 spectra were generated for original spectrum of each concentration and a comprehensive set of 10,000 spectra was ultimately obtained. This enhances the richness and diversity of the dataset for robust model training.

2.5.2. Spectral data preprocessing and partition

Spectral data inherently harbor various artifacts unrelated to sample information, such as fluorescence background, light scatter effects, and instrumental noise. Thus, preprocessing spectral data becomes imperative to eliminate uncertainties arising from these artifacts during the training process, thereby enhancing the model's generalization. To address this, we adopted a spectral preprocessing pipeline comprising three key steps: (1) smoothing, the Savitzky-Golay (S-G) smoother (window length = 7, polynomial fitting order = 3) was employed for spectral smoothing; (2) baseline correction, this step used polynomial fitting method to fit and calculate residual values for determining baseline; (3) normalization, the maximum-minimum normalization method was applied for data standardization by converting maximum and minimum values to the range [0,1].

After preprocessing the spectra, the spectra were proportionally divided into three segments: 81 % serves as the training set for convolutional neural network training; 9 % functions as the validation set for parameter verification and adjustment during training; the remaining 10 % is designated as the test set to evaluate neural network performance.

2.5.3. 1D CNN model for SERS data analysis

The 1D CNN regression model based on the LeNet-5 architecture was constructed to predict the concentration of MG residues [42]. The proposed 1D CNN architecture consists of an input layer, 2 convolutional layers, 2 max-pooling layers, 2 dense layers, and an output layer. In the model, the Raman features from the MG spectrum were flattened into a one-dimensional vector (432 × 1). This vector encapsulates the peak positions, shapes, and intensities of the characteristic peaks present in the spectrum. By maintaining and utilizing these Raman features with precision, the 1D CNN model can be effectively trained. In each convolutional layer, ReLU was used as activation function. To prevent over-

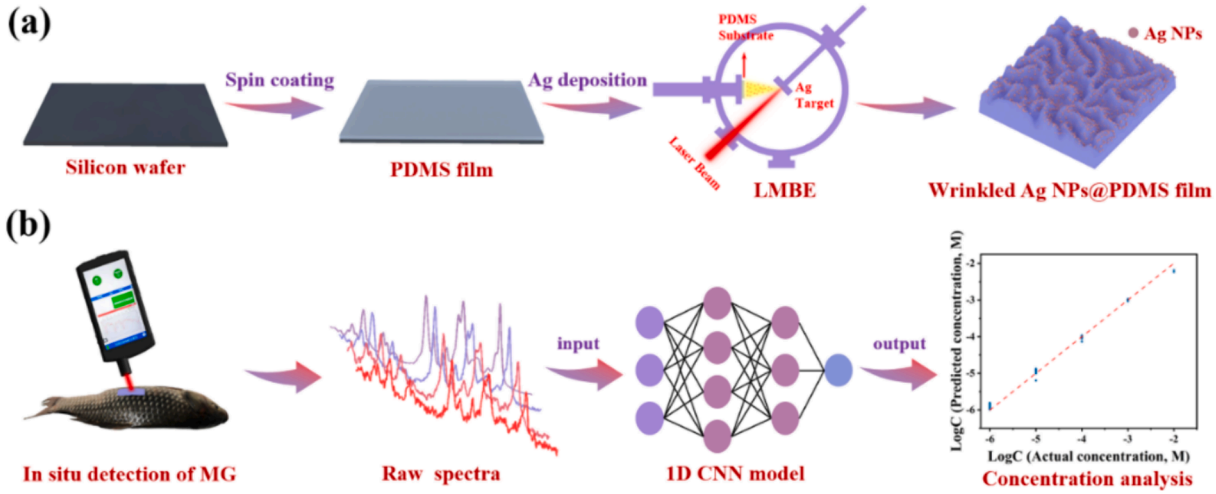


Fig. 1. Schematic illustration of the POCT platform for rapid quantitative analysis of MG in fish based on SERS and 1D CNN: (a) the preparation process of the wrinkled Ag NPs@PDMS film, (b) portable in situ detection measurement and deep learning analysis for concentration prediction.

fitting, dropout operation was used in the two dense layers. A linear activation function was used in the output layer. The architecture of the 1D CNN regression model is shown in Table S1.

For the CNN regression models, the Huber loss was employed as a loss function, as shown in equation (1) [43]:

$$L_\delta(y,y') = \begin{cases} \frac{1}{2}(y-y')^2, |y-y'| \leqslant \delta \\ \delta|y-y'| - \frac{1}{2}\delta^2, o.w. \end{cases} \quad (1)$$

where y represents the true value,y' is the predicted value, and δ is the hyperparameter of the Huber loss function. In this study, δ was set to 2 for Huber Loss. The initial learning rate and training iterations are established at 0.001 and 100 epochs, respectively. The batch size was set to 32. The adaptive moment estimation (Adam) was used as the optimizer. The model utilized the Keras framework and was implemented based on TensorFlow.

The model's predictive performance was assessed using the R^2, as shown in equation (2) [44].

$$R^2 = 1 - \frac{\sum_{n=1}^{N}(y_n - y_n')^2}{\sum_{n=1}^{N}(y_n - \bar{y})^2} \quad (2)$$

where y_n is the true value,y_n' represents the predicted value, and $\bar{y}$ denotes the mean of the true values.

Mean square error (MSE) is a metric commonly used for error analysis. It quantifies the average squared deviation between predicted and actual values. The MSE can be calculated using the equation (3) [45].

$$MSE = \frac{1}{N}\sum_{i=1}^{n}(y_i' - y_i)^2 \quad (3)$$

where y_i' denotes the predicted value,y_i represents the true value, and N is the number of samples.

3. Results and discussion

3.1. Fabrication and characterization of the wrinkled Ag NPs@PDMS film

To achieve sensitive in situ SERS detection of target molecules in complex samples and avoid complicated pre-treatment steps, the construction of high-density and easily accessible hot spots on the flexible substrate is of paramount importance. Here, we used a simple and convenient method to prepare the flexible and transparent SERS substrate by depositing a silver (Ag) film onto a PDMS film through LMBE

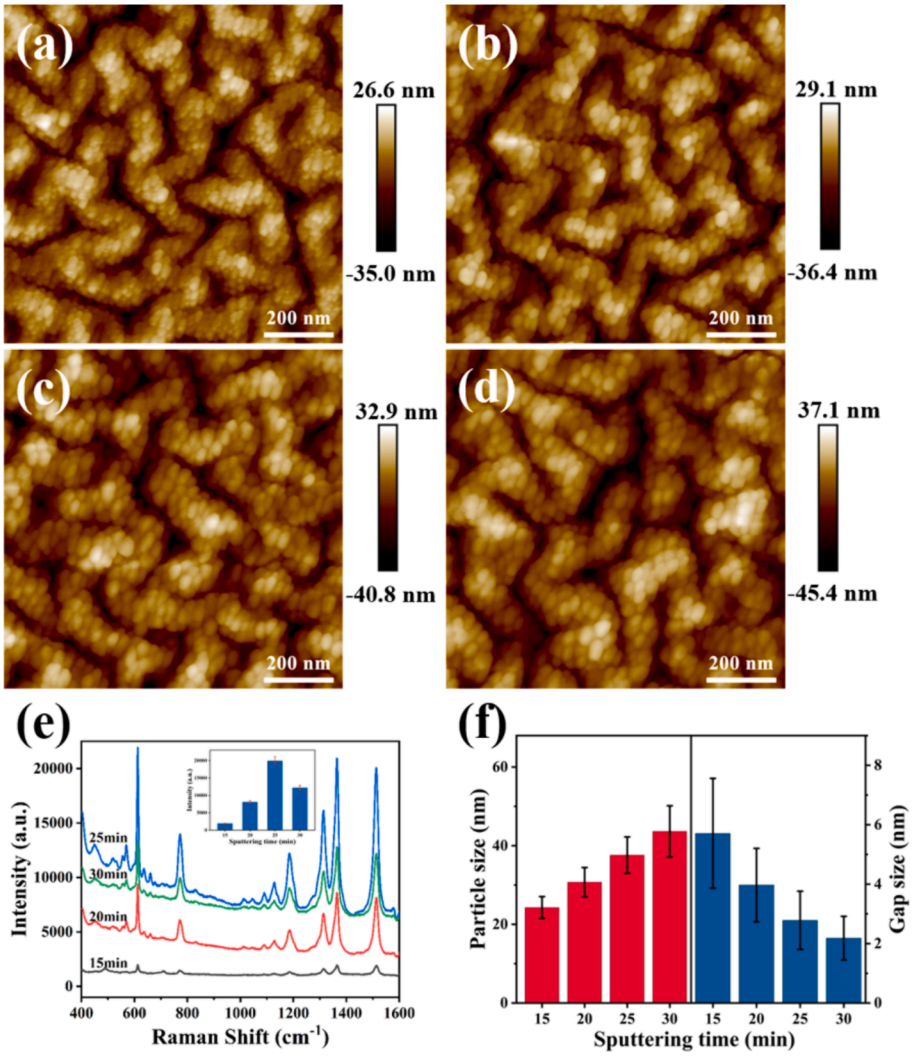


Fig. 2. AFM images of Ag-coated PDMS films with the deposition time of (a) 15 min, (b) 20 min, (c) 25 min, and (d) 30 min. (e) SERS spectra of 10^{-5} M R6G obtained from different Ag NPs@PDMS films. The inset shows the relationship between SERS intensity at 1510 cm^{-1} and the different sputtering times. (f) The histogram of the particle size and nanogaps size distribution for four different substrates.

deposition [46]. Fig. 2a-d present typical AFM images of the surface morphologies of Ag films with varying deposition times (from 15 to 30 min). Intriguingly, all as-deposited Ag films exhibit intricate labyrinth-like patterns of wrinkles. Notably, the AFM images revealed a substantial number of Ag nanoparticles (Ag NPs) dispersed randomly on these micro-scale wrinkles. A detailed examination of the surface morphology through SEM (Fig. S2), further corroborates the presence of Ag NPs on these micro-scale wrinkles. Furthermore, the low-magnification SEM images (Fig. S3) show that the Ag NPs are uniformly distributed. During the deposition process, the metal atoms sputtered with high kinetic energy have a propensity to coalesce into Ag NPs on the PDMS surface. The rise in temperature of the PDMS substrate, attributed to particle bombardment and heat radiation from the heating source, induces thermal expansion in the film/substrate system. Upon cooling to room temperature, the PDMS substrates contract, generating compressive stress at the interfaces due to the coefficient of thermal expansion mismatch between the Ag films and PDMS substrates. As this compressive stress surpasses a critical threshold, Ag NPs form on the randomly oriented wrinkles [47]. This ingenious approach not only yields a flexible SERS substrate but also capitalizes on the creation of a myriad of Ag NPs, providing high-density and easily accessible hot spots for enhanced sensitivity and uniformity in SERS detection.

To verify the relationship between deposition time and SERS enhancement effect, the SERS activity of the wrinkled Ag NPs@PDMS films was systematically examined using 10^{-5} M R6G as the probe molecule. Fig. 2e illustrates the SERS spectra of R6G collected on these Ag NPs@PDMS films with varying Ag-sputtering durations. Notably, the SERS intensity of the substrates exhibited a gradual increase within the Ag-sputtering duration range of 15 to 25 min, followed by a decrease with further elongation of the Ag-sputtering duration (as depicted in the inset of Fig. 2e). This observed variation in SERS activity aligns with the morphological evolution of the wrinkled Ag NPs@PDMS films at different Ag-sputtering durations. To delve deeper into the size and morphology of Ag NPs, a statistical analysis based on 100 measurements was conducted, as depicted in Fig. 2f. The histogram derived from AFM images revealed the particle sizes of the Ag NPs corresponding to different deposition times: 24.284 ± 2.771 nm, 30.722 ± 3.723 nm, 37.614 ± 4.612 nm, and 43.652 ± 6.496 nm, respectively. Furthermore, the interparticle distances between the Ag NPs were found to be 5.710 ± 1.849 nm, 3.970 ± 1.234 nm, 2.784 ± 0.980 nm, and 2.184 ± 0.733 nm, respectively. The above results demonstrate that the SERS substrate prepared with a larger Ag-sputtering duration yields a stronger SERS signal. This enhancement can be attributed to the increased number of effective and available hot spots for signal amplification. However, further extension of duration will lead to a decrease in the number of hot spots per unit irradiation volume, generating weakened SERS enhancement. Thus, the Ag NPs@PDMS film prepared with the deposition time of 25 min was used for all subsequent SERS measurements, due to its relatively high enhancement performance.

3.2. Performance evaluation of the wrinkled Ag NPs@PDMS film

Following structural optimization, the detection sensitivity of the prepared Ag NPs@PDMS film was assessed using various concentrations of R6G. Fig. 3a presents the SERS spectra of R6G with different concentrations ranging from 10^{-3} M to 10^{-7} M. Even at the low concentration of 10^{-7} M, the main Raman bands of R6G remained distinctly identifiable. In addition, the blank Raman spectra of Ag NPs@PDMS film was collected. It can be observed that the background signal from the Ag NPs@PDMS film was negligible, ensuring low interference with the determination of target molecules. Fig. 3b illustrates the plot of SERS intensity at peak 1510 cm^{-1} against the logarithm of R6G concentration, yielding a correlation coefficient (R^2) of 0.953. This high correlation underscores the potential of the wrinkled Ag NPs@PDMS film for quantitative molecular analysis. Furthermore, the analytical enhancement factor (AEF) for the optimized Ag NPs@PDMS film was calculated using the following equation [48]:

$$AEF = \frac{I_{SERS}/C_{SERS}}{I_{Raman}/C_{Raman}} \quad (4)$$

where the I_{SERS} and I_{Raman} were the Raman intensities of R6G at 1510 cm^{-1} obtained from the Ag NPs@PDMS film and the pure PDMS film, respectively. C_{SERS} and C_{Raman} represented the corresponding concentrations of R6G on the Ag NPs@PDMS film and the pure PDMS film, respectively. The intensity I_{SERS} for 10^{-7} M R6G on the Ag NPs@PDMS film is ~3919, and the intensity I_{Raman} for 10^{-3} M R6G on the pure PDMS film is ~310, as shown in Fig. S4. Therefore, the AEF was calculated to be 1.26 × 10^5. The high SERS activity of the optimized Ag NPs@PDMS film was primarily attributed to the abundance of hot spots on the substrate. These hot spots can be generated in the nanogaps between neighboring Ag NPs on a single wrinkle as well as across adjacent wrinkles. Additionally, the wrinkled surface increased the density of hot spots and the number of molecules within the detection volume, collectively contributing to the high SERS enhancement.

Evaluating SERS substrates for practical applications necessitates a keen focus on two pivotal aspects: reproducibility and storage stability. To investigate the point-to-point reproducibility of the Ag NPs@PDMS film, SERS spectra of R6G at a concentration of 10^{-6} M were collected from 10 randomly selected sites on the same substrate, as illustrated in Fig. S5. The corresponding relative standard deviation (RSD) of Raman intensities at 1510 cm^{-1} was 7.55 %, as shown in Fig. 4a. Additionally, SERS mapping of R6G at 1510 cm^{-1} in a 30 × 30 μm^2 area was performed (Fig. 4b). The RSD value evaluated across the 900 points was 7.95 %. These results revealed the substrate's commendable uniformity. Moreover, to assess batch-to-batch reproducibility, SERS spectra of R6G were gathered from 5 different batches, with 5 random sites selected for each batch (Fig. S6). The statistical analysis of Raman intensities at 1510 cm^{-1} exhibited a low RSD value of 2.42 % (Fig. 4c), demonstrating the excellent reproducibility of the Ag NPs@PDMS films. The good

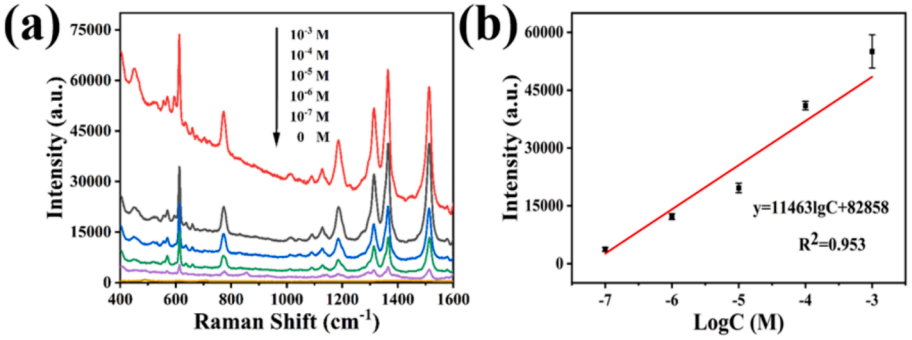


Fig. 3. (a) SERS spectra of R6G with different concentrations collected from the wrinkled Ag NPs@PDMS film. (b) SERS intensity at 1510 cm^{-1} as a function of the R6G concentration.

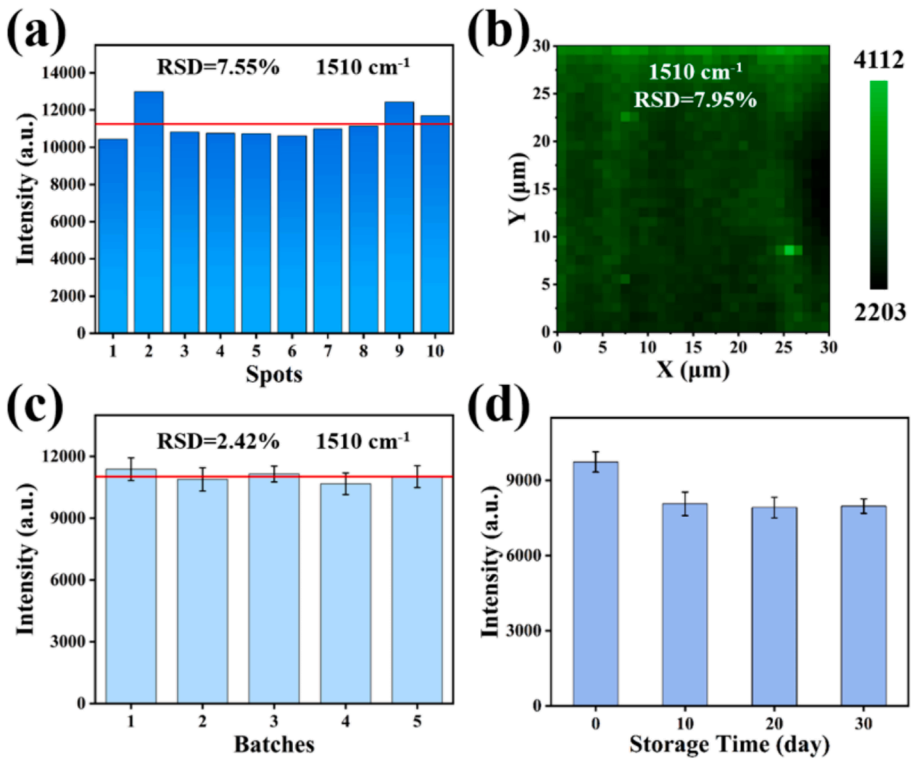


Fig. 4. (a) SERS intensity of R6G (10^{-6} M) at 1510 cm^{-1} collected from 10 random spots on the Ag NPs@PDMS film. (b) Raman mapping of R6G (10^{-6} M) at 1510 cm^{-1} detected on the Ag NPs@PDMS film. (c) SERS intensity of R6G (10^{-6} M) at 1510 cm^{-1} recorded from 5 different Ag NPs@PDMS films. (d) SERS intensity of R6G (10^{-6} M) at 1510 cm^{-1} recorded from different storage stages.

uniformity and reproducibility of the Ag NPs@PDMS films were ascribed to the controllable and reproducible preparation process. Table S2 presents a comparison of the sensing performance of the wrinkled Ag NPs@PDMS substrate with other flexible SERS substrates. While our substrate may exhibit slightly lower enhancement compared to other alternatives, it excels in terms of uniformity and reproducibility. This characteristic renders it an optimal selection for achieving consistent Raman spectra via an in situ detection method, leading to dependable Raman data for the development, validation, and application of 1D CNN model. Additionally, the straightforward preparation process of our substrate allows for mass production of flexible and transparent SERS substrates on a large scale. To evaluate the storage stability of this substrate under indoor storage condition, Raman measurements of R6G on the wrinkled Ag NPs@PDMS film were performed at 10-day intervals over a span of 30 days (Fig. S7). Fig. 4d illustrates the evolving trend in SERS intensity at 1510 cm^{-1} over the storage period. The Raman intensity exhibited an initial decrease, followed by stabilization. Even after 30 days, the SERS intensity still maintained ~ 82 % of the original, affirming its good storage stability. Thus, the above results indicate that the wrinkled Ag NPs@PDMS film can be used as a reliable and stable SERS platform for practical applications.

Considering the remarkable flexibility and transparency of the PDMS film, the Ag NPs@PDMS film holds substantial potential as a SERS substrate for in situ detection on irregular surfaces. Thus, it is vital to evaluate the mechanical robustness of this substrate. This was achieved by examining the impact of cyclic deformations on the variation of SERS activity. The SERS spectra of R6G molecules on the Ag NPs@PDMS films under bending and torsion tests were shown in Fig. 5a and 5c, respectively. Notably, the corresponding SERS intensities at 1510 cm^{-1} exhibited only slight weakening after up to 100 cycles of bending and torsion, as evidenced in Fig. 5b and 5d. These results illuminate that the Ag NPs@PDMS films possess the remarkable ability to withstand mechanical deformations, aligning with the demands of a wearable sensor. The stable fixation of Ag NPs on the PDMS surface was identified as a contributing factor to this mechanical resilience. To delve deeper into the adhesion between the Ag NPs and PDMS, a scotch-tape peel test was executed. Fig. 5e portrays the SERS spectra of R6G on the flexible Ag NPs@PDMS film after three repeated peel tests. Remarkably, even after these tests, the flexible Ag NPs@PDMS film maintained a stable SERS intensity of R6G at 1510 cm^{-1} (Fig. 5f). This result demonstrated the effective adhesion between Ag NPs and PDMS, reinforcing the credibility of the flexible Ag NPs@PDMS film for practical applications. Thus, according to the above results, the as-developed substrate offered several distinct advantages: high-density and highly accessible hot spots on the PDMS surface; good adhesion between the Ag NPs and PDMS, in situ detection capability; simple and convenient preparation process.

3.3. *Rapid in situ detection of MG residues on fish scales*

The study conducted by W.-L. Fan et al. provided valuable insights into the utilization of SERS sensors for detecting MG contamination on live fish skin [49]. In their research, a novel flexible SERS sensor was designed using chewing gum, enabling rapid sampling and detection of MG on live fish skin for a more accurate assessment of contamination levels. The flexibility and viscoelasticity of the chewing gum allowed for direct sampling of minute amounts of MG on the fish skin. In comparison to the peel-off sampling method, in situ detection approach allows for real-time monitoring of chemical compounds on surfaces without the need for sample collection, making it particularly advantageous in situations requiring quick detection and identification of substances. Additionally, research by Chowdhury et al. showed that the adsorption of MG onto fish scales (Labeo rohita) was spontaneous due to the negative values of Gibbs free energies [50]. Investigating the distribution of MG on fish scales can offer valuable insights into potential risks associated with contamination.

The wrinkled Ag NPs@PDMS film exhibited exceptional flexibility and transparency (Fig. 6a), which improves the maneuverability of the substrate, making it easy to operate in situ determination on curved

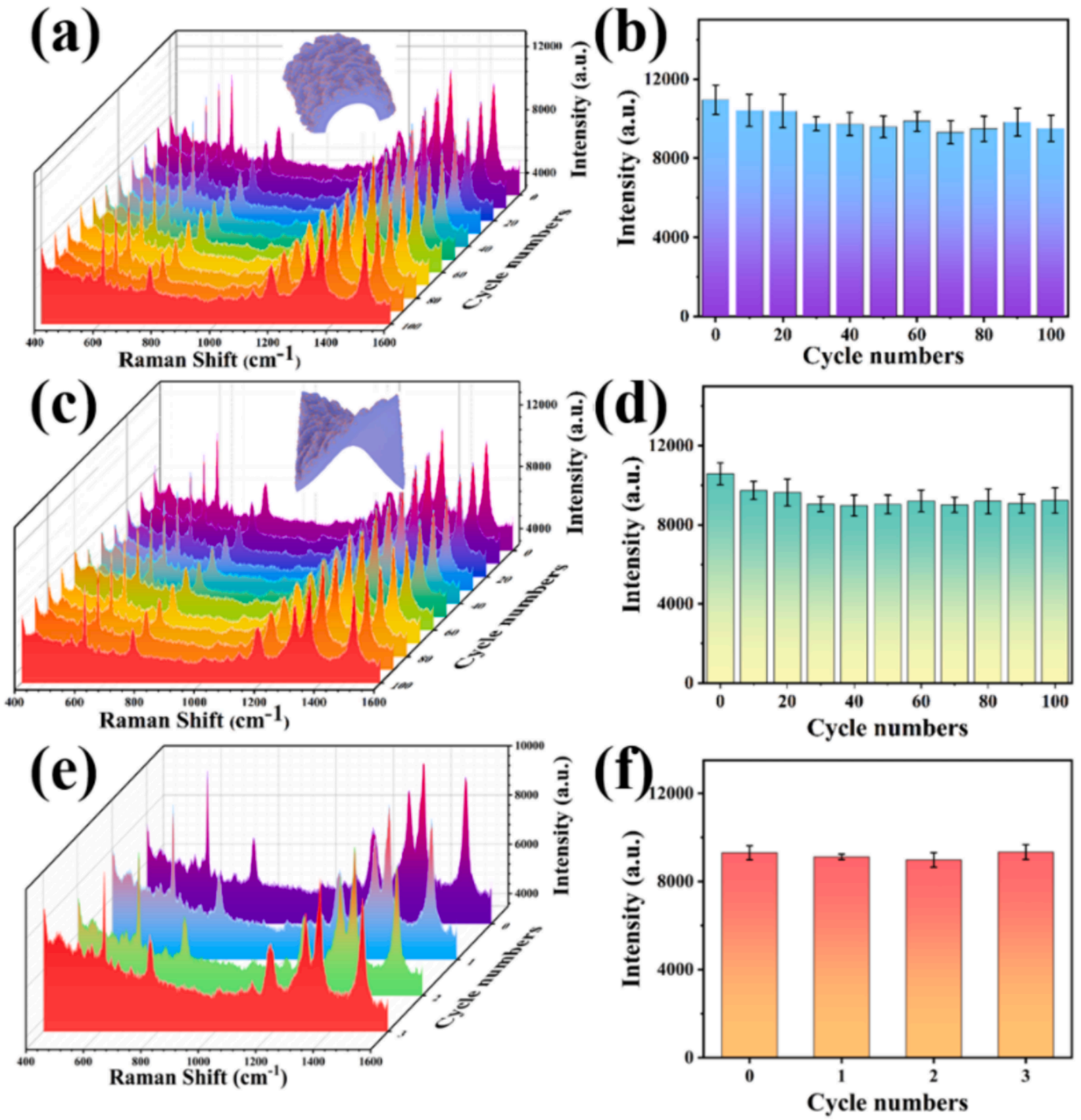


Fig. 5. (a) SERS spectra of R6G (10^{-6} M) and (b) corresponding signal intensity at 1510 cm^{-1} in the bending test. (c) SERS spectra of R6G (10^{-6} M) and (d) corresponding signal intensity at 1510 cm^{-1} in the twisting test. (e) SERS spectra of R6G (10^{-6} M) and (f) corresponding signal intensity at 1510 cm^{-1} in the adhesion test.

surfaces. To validate this concept, we used the fabricated Ag NPs@PDMS film to directly measure MG on fish scales. In the experiment, 20 μL of MG solutions with different concentrations ranging from 10^{-2} to 10^{-6} M were added to the surface of a fish skin. After natural drying, the prepared flexible and transparent SERS substrate was placed on the fish scales, ensuring contact between Ag NPs and the skin, and the SERS signals were collected by a portable Raman spectrometer (Fig. 6b). The obtained Raman characteristic bands of MG were consistent with the previous report [15], and discernible even at a concentration as low as 10^{-6} M (Fig. 6c). The calibration curve in Fig. 6d revealed a robust linear relationship ($R^2 = 0.982$) between the SERS intensity at 1616 cm^{-1} and the logarithmic concentration of MG. The above results demonstrate that the wrinkled Ag NPs@PDMS film can act as a flexible and transparent SERS substrate, which can be handily applied in daily life by means of in situ detection combining with a portable Raman spectrometer.

3.4. Quantification analysis of MG residues using 1D CNN

The introduction of CNN into the quantification of SERS spectra

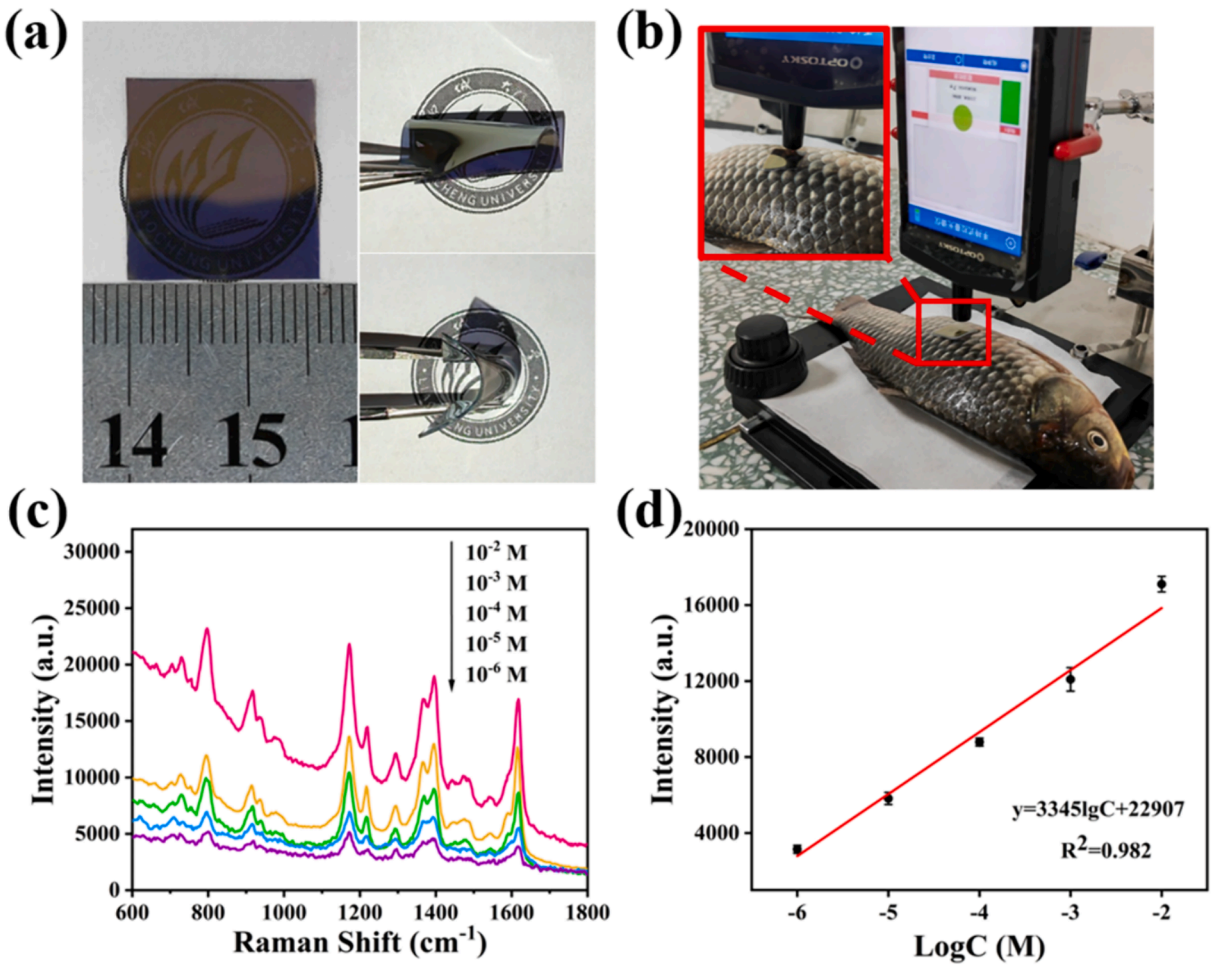


Fig. 6. (a) The transparency and flexibility of the wrinkled Ag NPs@PDMS film. (b) The photography in the SERS measurement process. (c) SERS spectra of MG (10^{-2}-10^{-6} M) on the fish scales. (d) Calibration curve plotted between the average peak intensity at 1616 cm^{-1} against the logarithmic concentration of MG.

holds great promise for advancing SERS technology as a POCT platform. Here, a 1D CNN qualitative analysis model was constructed to predict MG concentrations by analyzing concentration-dependent spectra. The schematic diagram of the operation of the 1D CNN model is illustrated in Fig. 7a, which is aimed for establishing concentration calibration curves based on logarithms of concentrations. Neural networks are prone to overfitting the training data, leading to poor performance on the testing or validation data set. The learning curves can be used to assess the model's performance. Fig. 7b depicts the loss curves for the 1D CNN model on both the training and validation sets. Over the course of 100 iterations, it can be observed that the loss curves rapidly decline to a lower level and subsequently maintain stability without significant fluctuations. This indicates that the model has achieved an optimal state. Also, R^2 values of the 1D CNN model in the training step and validation step is shown in Fig. 7c. The R^2 increased to a higher level for both training step and validation step, and rose to a stable value of 0.997 after 46 epochs on the validation set, indicating its proficient capability for quantitative analysis. The regression result of the predicted concentration (C_{pre}) and the actual concentration (C_{act}) from the 1D CNN model was presented in a log–log scale (Fig. 7d). The C_{pre} aligned well with the C_{act}, yielding a low MSE value of 0.0104 and a high R^2 value of 0.9947, which indicates that the developed 1D CNN model has excellent quantitative performance.

In this study, we have demonstrated the successful integration of SERS technology with 1D CNN for the rapid detection and quantitative analysis of pollutants, representing a significant advancement in the field of POCT. However, there exist several potential drawbacks and limitations that must be addressed in future research endeavors. One primary challenge is the establishment of standardized protocols and guidelines for conducting SERS measurements, as variations in experimental conditions and equipment settings can introduce inconsistencies in results, thus impeding the reproducibility and comparability of outcomes across different studies. Additionally, the reliance on data-driven approaches for data analysis in SERS studies may be constrained by the availability of high-quality training data, potentially leading to inaccuracies in model predictions. Moreover, CNN models developed using specific datasets may not always be readily transferable to novel experimental conditions or sample types, thereby restricting the practical utility of data-driven Raman spectroscopy in real-world scenarios. To overcome these limitations, future research efforts should focus on standardizing methodologies, enhancing the availability of high-quality training data, and improving the transferability of CNN models across different experimental conditions and sample types. By addressing these challenges, researchers can improve the reliability and applicability of data-driven Raman spectroscopy, thereby facilitating its widespread adoption in practical applications.

4. Conclusions

We prepared a flexible and transparent SERS substrate made of the wrinkled Ag NPs@PDMS film that enabled in situ detection on curved surfaces. Morphological characterization of the wrinkled Ag NPs@PDMS film indicated that abundant hot spot formation inside the rolling and undulating Ag NPs. After confirming the high SERS

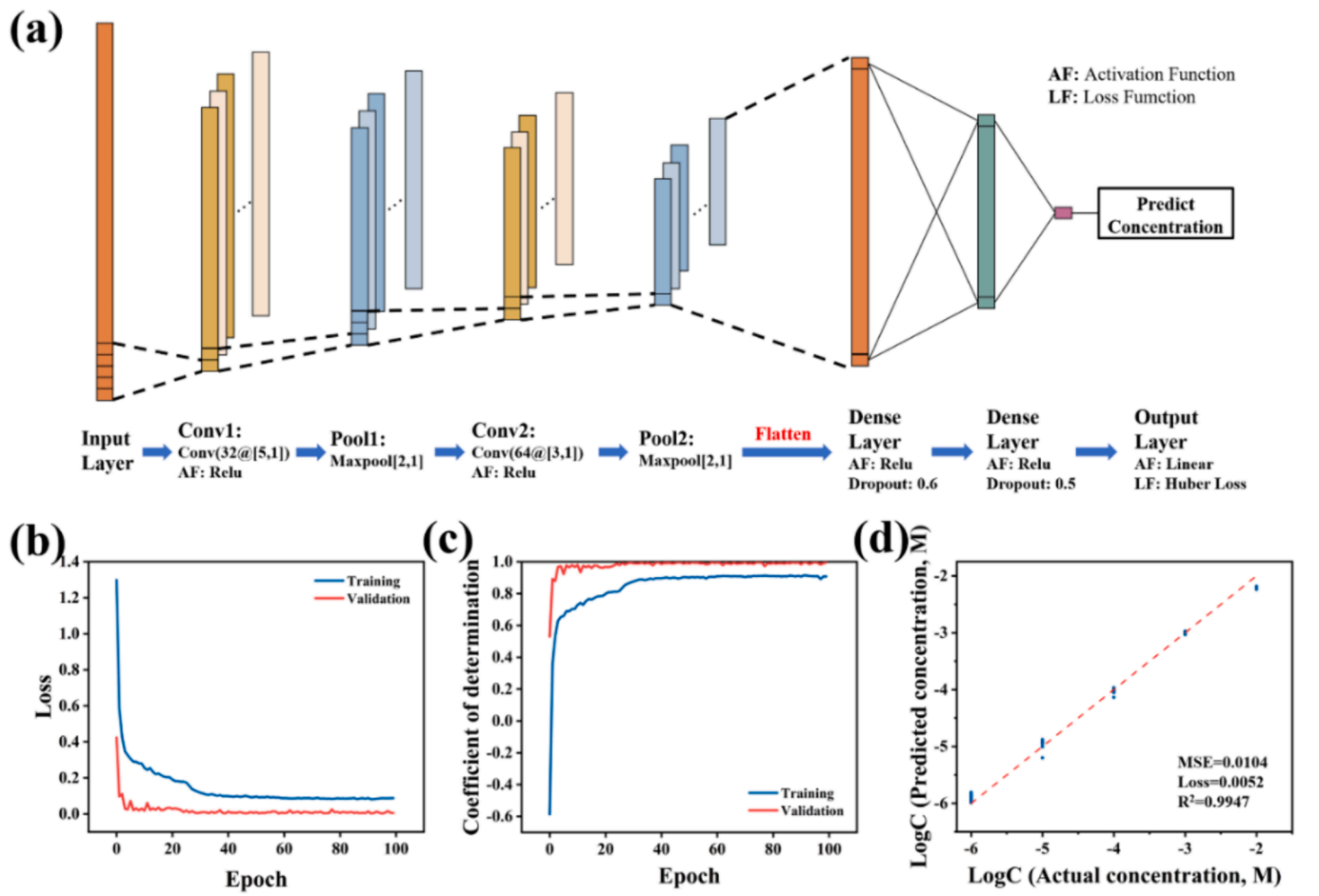


Fig. 7. (a) The architecture of 1D CNN quantitative analysis model. (b) Loss curves of 1D CNN model on training set and validation set. (c) R^2 values for training and validation steps in the 1D CNN model. (d) The linear regression plot of the predication set in the 1D CNN model.

activity, good reproducibility, outstanding mechanical stability of the wrinkled Ag NPs@PDMS film, it was integrated with a handheld Raman spectrometer for developing an onsite applicable MG detection system, which can achieve convenient and rapid detection of MG residues on fish scales without complex sample pretreatment and detection procedures. For rapid quantitation of MG concentrations, a 1D CNN quantitative analysis model was developed. The results demonstrated that the 1D CNN model had outstanding predictive capability, achieving an impressive MSE of 0.0104 and an R^2 of 0.9947. Therefore, the established POCT platform, harmonizing a flexible and transparent SERS substrate, a portable Raman spectrometer, and a 1D CNN quantitative analysis model, offers a robust on-site, real-time detection method with expansive potential applications in related fields.

CRediT authorship contribution statement

Zhaoyi Zhang: Visualization, Methodology, Investigation. **Hefu Li:** Writing – original draft, Validation, Supervision, Funding acquisition. **Lili Huang:** Investigation, Formal analysis. **Hongjun Wang:** Visualization, Data curation. **Huijuan Niu:** Funding acquisition, Formal analysis. **Zhenshan Yang:** Writing – review & editing. **Minghong Wang:** Supervision, Conceptualization.

Declaration of competing interest

The authors declare that they have no known competing financial interests or personal relationships that could have appeared to influence the work reported in this paper.

Data availability

Data will be made available on request.

Acknowledgements

This work was supported by Shandong Provincial Natural Science Foundation (ZR2021MF097, ZR2022MF305); Liaocheng University Start-up Fund for Doctoral Scientific Research (318051542).

Appendix A. Supplementary material

Supplementary data to this article can be found online at https://doi.org/10.1016/j.saa.2024.124655.

References

[1] S.J. Culp, F.A. Beland, Malachite green: a toxicological review, J. Am. Coll. Toxicol. 15 (1996) 219–238.
[2] F. Wang, H. Wang, Y.-D. Shen, Y.-J. Li, J.-X. Dong, Z.-L. Xu, J.-Y. Yang, Y.-M. Sun, Z.-L. Xiao, Bispecific monoclonal antibody-based multianalyte ELISA for furaltadone metabolite, malachite green, and leucomalachite green in aquatic products, J. Agric. Food Chem. 64 (2016) 8054–8061.
[3] A.A. Fallah, A. Barani, Determination of malachite green residues in farmed rainbow trout in Iran, Food Control 40 (2014) 100–105.
[4] A.A. Bergwerff, P. Scherpenisse, Determination of residues of malachite green in aquatic animals, J. Chromatogr. B 788 (2003) 351–359.
[5] L. Wu, Z.-Z. Lin, H.-P. Zhong, X.-M. Chen, Z.-Y. Huang, Rapid determination of malachite green in water and fish using a fluorescent probe based on CdTe quantum dots coated with molecularly imprinted polymer, Sens. Actuators, B 239 (2017) 69–75.

[6] J. Langer, D. Jimenez de Aberasturi, J. Aizpurua, et al., Present and future of surface-enhanced Raman scattering, ACS Nano 14 (2020) 28–117.
[7] L. Jiang, M.M. Hassan, S. Ali, H. Li, R. Sheng, Q. Chen, Evolving trends in SERS-based techniques for food quality and safety: A review, Trends Food Sci. Technol. 112 (2021) 225–240.
[8] A.G. Mukherjee, K. Renu, A.V. Gopalakrishnan, V.P. Veeraraghavan, S. Vinayagam, S. Paz-Montelongo, A. Dey, B. Vellingiri, A. George, H. Madhyastha, R. Ganesan, Heavy metal and metalloid contamination in food and emerging technologies for its detection, Sustainability 15 (2023) 1195.
[9] M.T. Yaraki, A. Tukova, Y. Wang, Emerging SERS biosensors for the analysis of cells and extracellular vesicles, Nanoscale 14 (2022) 15242–15268.
[10] S.-Y. Ding, E.-M. You, Z.-Q. Tian, M. Moskovits, Electromagnetic theories of surface-enhanced Raman spectroscopy, Chem. Soc. Rev. 46 (2017) 4042–4076.
[11] L. Wu, L. Cui, J. Guo, Y. Peng, J. Zou, B. Yu, L. Qian, Rapid and flexible construction of inverted silicon architectures with nanogaps as high-performance SERS substrates, Appl. Surf. Sci. 594 (2022) 153429.
[12] L. Ouyang, L. Yao, T. Zhou, L. Zhu, Accurate SERS detection of malachite green in aquatic products on basis of graphene wrapped flexible sensor, Anal. Chim. Acta 1027 (2018) 83–91.
[13] G. Yang, X. Fang, Q. Jia, H. Gu, Y. Li, C. Han, L.-L. Qu, Fabrication of paper-based SERS substrates by spraying silver and gold nanoparticles for SERS determination of malachite green, methylene blue, and crystal violet in fish, Microchim. Acta 187 (2020) 310.
[14] L. Zhang, J. Liu, G. Zhou, Z. Zhang, Controllable in-situ growth of silver nanoparticles on filter paper for flexible and highly sensitive SERS sensors for malachite green residue detection, Nanomaterials 10 (2020) 826.
[15] X. Tian, Q. Fan, J. Guo, Q. Yu, L. Xu, X. Kong, Surface-enhanced Raman scattering of flexible cotton fiber-Ag for rapid adsorption and detection of malachite green in fish, Spectrochim. Acta Part A Mol. Biomol. Spectrosc. 263 (2021) 120174.
[16] L. Xie, H. Zeng, J. Zhu, Z. Zhang, H. Sun, W. Xia, Y. Du, State of the art in flexible SERS sensors toward label-free and onsite detection: From design to applications, Nano Res. 15 (2022) 4374–4394.
[17] Z. Li, X. Huang, G. Lu, Recent developments of flexible and transparent SERS substrates, J. Mater. Chem. C 8 (2020) 3956–3969.
[18] D. Zhang, H. Pu, L. Huang, D.W. Sun, Advances in flexible surface-enhanced Raman scattering (SERS) substrates for nondestructive food detection: Fundamentals and recent applications, Trends Food Sci. Tech. 109 (2021) 690–701.
[19] J. Chen, M. Huang, L. Kong, Flexible Ag/nanocellulose fibers SERS substrate and its applications for in-situ hazardous residues detection on food, Appl. Surf. Sci. 533 (2020) 147454.
[20] L.-B. Zhong, J. Yin, Y.-M. Zheng, Q. Liu, X.-X. Cheng, F.-H. Luo, Self-assembly of Au nanoparticles on PMMA template as flexible, transparent, and highly active SERS substrates, Anal. Chem. 86 (2014) 6262–6267.
[21] X. Fan, H. Zhang, X.R. Zhao, K. Lv, T. Zhu, Y. Xia, C. Yang, C. Bai, Three-dimensional SERS sensor based on the sandwiched G@ AgNPs@ G/PDMS film, Talanta 233 (2021) 122481.
[22] L. Li, W.S. Chin, Rapid fabrication of a flexible and transparent Ag nanocubes@ PDMS film as a SERS substrate with high performance, ACS Appl. Mater. Interfaces 12 (2020) 37538–37548.
[23] H. Zhang, N. Zhao, H. Li, M. Wang, X. Hao, M. Sun, X. Li, Z. Yang, H. Yu, C. Tian, C. Wang, 3D flexible SERS substrates integrated with a portable Raman analyzer and wireless communication for point-of-care application, ACS Appl. Mater. Interfaces 14 (2022) 51253–51264.
[24] M. Sun, H. Zhang, H. Li, X. Hao, C. Wang, L. Li, Z. Yang, C. Tian, Ag microlabyrinth/nanoparticles coated large-area thin PDMS films as flexible and transparent SERS substrates for in situ detection, Spectrochim. Acta Part A Mol. Biomol. Spectrosc. 303 (2023) 123153.
[25] A. Alyami, A.J. Quinn, D. Iacopino, Flexible and transparent Surface Enhanced Raman Scattering (SERS)-Active Ag NPs/PDMS composites for in-situ detection of food contaminants, Talanta 201 (2019) 58–64.
[26] X. Ma, J. Xie, Z. Wang, Y. Zhang, Transparent and flexible AuNSs/PDMS-based SERS substrates for in-situ detection of pesticide residues, Spectrochim. Acta Part A Mol. Biomol. Spectrosc. 267 (2022) 120542.
[27] Y. Wang, Z. Wang, C. Chen, J. Liu, J. Lu, N. Lu, Fabrication of flexible pyramid array as SERS substrate for direct sampling and reproducible detection, Anal. Chem. 95 (2023) 14184–14191.
[28] S.-H. Luo, W.-L. Wang, Z.-F. Zhou, Y. Xie, B. Ren, G.-K. Liu, Z.-Q. Tian, Visualization of a machine learning framework toward highly sensitive qualitative analysis by SERS, Anal. Chem. 94 (2022) 10151–10158.
[29] S. Yan, C. Liu, S. Fang, J. Ma, J. Qiu, D. Xu, L. Li, J. Yu, D. Li, Q. Liu, SERS-based lateral flow assay combined with machine learning for highly sensitive quantitative analysis of Escherichia coli O157: H7, Anal. Bioanal. Chem. 412 (2020) 7881–7890.
[30] Y. Yang, B. Xu, J. Murray, J. Haverstick, X. Chen, R.A. Tripp, Y. Zhao, Rapid and quantitative detection of respiratory viruses using surface-enhanced Raman spectroscopy and machine learning, Biosens. Bioelectron. 217 (2022) 114721.
[31] R. Beeram, D. Banerjee, L.M. Narlagiri, V.R. Soma, Machine learning for rapid quantification of trace analyte molecules using SERS and flexible plasmonic paper substrates, Anal. Methods 14 (2022) 1788–1796.
[32] B. Debus, H. Parastar, P. Harrington, D. Kirsanov, Deep learning in analytical chemistry, TrAC-Trend Anal. Chem. 145 (2021) 116459.
[33] F.U. Ciloglu, A. Caliskan, A.M. Saridag, I.H. Kilic, M. Tokmakci, M. Kahraman, O. Aydin, Drug-resistant Staphylococcus aureus bacteria detection by combining surface-enhanced Raman spectroscopy (SERS) and deep learning techniques, Sci. Rep. 11 (2021) 18444.
[34] M. Qiu, L. Tang, J. Wang, Q. Xu, S. Zheng, S. Weng, SERS with flexible β-CD@ AuNP/PTFE substrates for in situ detection and identification of PAH residues on fruit and vegetable surfaces combined with lightweight network, Foods 12 (2023) 3096.
[35] S. Weng, W. Zhu, P. Li, H. Yuan, X. Zhang, L. Zheng, J. Zhao, L. Huang, P. Han, Dynamic surface-enhanced Raman spectroscopy for the detection of acephate residue in rice by using gold nanorods modified with cysteamine and multivariant methods, Food Chem. 310 (2020) 125855.
[36] J. Ding, Q. Lin, J. Zhang, G.M. Young, C. Jiang, Y. Zhong, J. Zhang, Rapid identification of pathogens by using surface-enhanced Raman spectroscopy and multi-scale convolutional neural network, Anal. Bioanal. Chem. 413 (2021) 3801–3811.
[37] J. Zhu, A.S. Sharma, J. Xu, Y. Xu, T. Jiao, Q. Ouyang, H. Li, Q. Chen, Rapid on-site identification of pesticide residues in tea by one-dimensional convolutional neural network coupled with surface-enhanced Raman scattering, Spectrochim. Acta Part A Mol. Biomol. Spectrosc. 246 (2021) 118994.
[38] Q. Wang, F. Pian, M. Wang, S. Song, Z. Li, P. Shan, Z. Ma, Quantitative analysis of Raman spectra for glucose concentration in human blood using Gramian angular field and convolutional neural network, Spectrochim. Acta Part A Mol. Biomol. Spectrosc. 275 (2022) 121189.
[39] M. Erzina, A. Trelin, O. Guselnikova, A. Skvortsova, K. Strnadova, V. Svorcik, O. Lyutakov, Quantitative detection of α1-acid glycoprotein (AGP) level in blood plasma using SERS and CNN transfer learning approach, Sens. Actuators, B 367 (2022) 132057.
[40] K. Georgouli, M.T. Osorio, J.M. Del Rincon, A. Koidis, Data augmentation in food science: Synthesising spectroscopic data of vegetable oils for performance enhancement, J. Chemom. 32 (2018) e3004.
[41] J. Zhu, X. Jiang, Y. Rong, W. Wei, S. Wu, T. Jiao, Q. Chen, Label-free detection of trace level zearalenone in corn oil by surface-enhanced Raman spectroscopy (SERS) coupled with deep learning models, Food Chem. 414 (2023) 135705.
[42] Y. Lecun, L. Bottou, Y. Bengio, P. Haffner, Gradient-based learning applied to document recognition, Proc. IEEE 86 (1998) 2278–2324.
[43] A. Esmaeili, F. Marvasti, A novel approach to quantized matrix completion using huber loss measure, IEEE Signal Proc. Let. 26 (2019) 337–341.
[44] S. Menard, Coefficients of determination for multiple logistic regression analysis, Am. Stat. 54 (2000) 17–24.
[45] Z. Wang, A.C. Bovik, Mean squared error: Love it or leave it? A new look at signal fidelity measures, IEEE Signal Pro. Mag. 26 (2009) 98–117.
[46] H. Li, N. Zhao, Y. Wang, R. Zou, Z. Yang, C. Zhu, M. Wang, H. Yu, Wafer-scale silver nanoislands with~5 nm interstitial gaps for surface-enhanced Raman scattering, Opt. Mater. Express 10 (2020) 3359–3371.
[47] K. Wu, H.Z. Yuan, S.J. Li, J.Y. Zhang, G. Liu, J. Sun, Two-stage wrinkling of Al films deposited on polymer substrates, Scr. Mater. 162 (2019) 456–459.
[48] M. Charconnet, M.T. Korsa, S. Petersen, J. Plou, C. Hanske, J. Adam, A. Seifert, Generalization of self-assembly toward differently shaped colloidal nanoparticles for plasmonic superlattices, Small Methods 7 (2023) 2201546.
[49] W.-L. Fan, S.-W. Yang, D.-M. Wang, Z.-J. Gong, M.-K. Fan, Screening for malachite green contamination on live fish skin with chewing gum based viscoelastic SERS sensor, J. Food Drug Anal. 28 (2020) 231–238.
[50] S. Chowdhury, P. Das Saha, U. Ghosh, Fish (Labeo rohita) scales as potential low-cost biosorbent for removal of malachite green from aqueous solutions, Biorem. J. 16 (2012) 235–242.